

Design and Implementation of a Test Procedure for the Evaluation of Interference Coupling in Magnetic Resonance Imaging

Bodo Gambal¹, Enrico Pannicke¹, Mathias Magdowski¹, Bennet Hensen², Frank Wacker² and Ralf Vick¹

Abstract—External therapy devices in the shielded room of a magnetic resonance tomograph (MRT) can cause radio frequency (RF) imaging artifacts, which renders the image useless for diagnosis or guiding the procedure. At present, there is no standard procedure to evaluate their conformity with MR imaging.

The aim of this paper is to adapt an already existing procedure from the electromagnetic compatibility (EMC), the reverberation chamber (RVC), to evaluate interferences in the magnetic resonance (MR) environment. For this purpose, a test rig was developed which is adapted to the special conditions of the MRI environment. In addition, the suitability of this procedure will be demonstrated in first measurements. The results show that the method can trace and evaluate RF interference of therapy devices. Moreover, the shielded cabin of an MRI system is suitable to perform such measurements.

I. INTRODUCTION

Due to numerous technical innovations and developments in medical technology, the range of applications of interventional magnetic resonance imaging (iMRI) in therapy and diagnosis is constantly expanding. Compared to conventional methods, MRI offers high soft tissue contrast images, which make it possible to visualize many tumors more clearly or at all. For this reason, iMRI is an established diagnosis and therapy support method, particularly for tumors [1].

For these types of therapies MR-compatible solutions are needed, especially because the therapy room is located directly in the MR cabin and simultaneous imaging is essential for the intervention. These therapeutic setups require additional equipment, for example, instruments and patient positioning solutions. In particular therapeutic devices can interfere with MR imaging, which is extremely susceptible to electromagnetic interference around the Larmor frequency [2]. It must therefore be ensured that the developed devices not only guarantee patient safety but also the safe conduct of the treatment. In order to ensure both during treatment, external devices must under no circumstances influence MR imaging [3].

A special problem of MRI is the influence of high-frequency emissions from external devices. The so called *zipper artifacts* are crossing the MR image in phase or frequency direction (see Fig. 1). The evaluation of these interference

for electromagnetic compatibility (EMC) must be included in the MR compatibility [4]. The analysis of special EMC environments by the manufacturers is required by the standard IEC60601-1-2, however, there are currently no normative specifications and no standardized test method either for analyzing devices interferences in the MR environment [3]. In general, standardized methods for disturbance evaluation should include the following properties [5]:

- Comparability of the results
- High reproducibility
- Reasonable effort

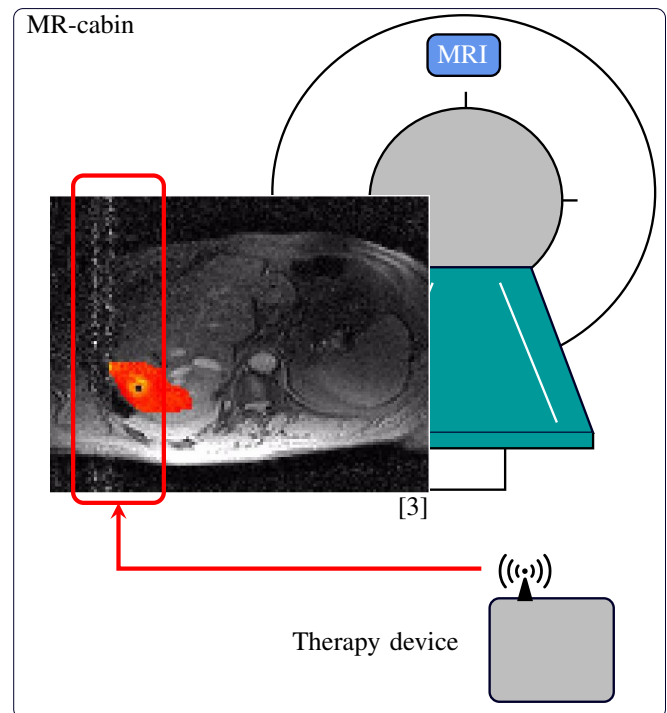


Fig. 1: MRI zipper artifacts due to emission by the therapy device in shielded cabin

II. STATE OF THE ART

Current test methods include visual inspection of the images, an analysis of the signal-to-noise ratio (SNR) and the received spectrum of the MRI. For this purpose, MR slice images are acquired with phantoms. The SNR is analyzed in the acquired slice images by analysing the region of interest (ROI). An example can be seen in Fig. 3. In the field of medical imaging the SNR is defined as the average

¹Bodo Gambal, Enrico Pannicke, Mathias Magdowski and Ralf Vick are with Faculty of Electrical Engineering and Information Technology, University of Magdeburg, Department of Electromagnetic Compatibility, Institute of Medical Technology, Otto-von-Guericke University, 39124 Magdeburg, Germany (email: bodo.gambal@ovgu.de).

²Bennet Hensen and Frank Wacker are with Department of Radiology, Medical College Hannover, 30625 Hannover, Germany (email: Hensen.Bennet@mh-hannover.de).

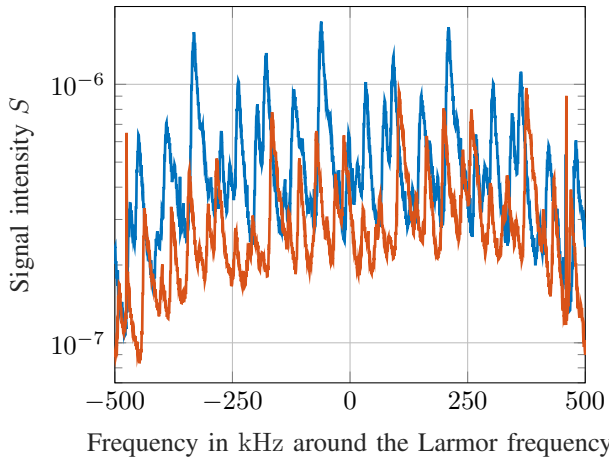


Fig. 2: Received spectrum at the MRI recorded for two different therapy device position

of the signal μ divided by the standard deviation σ of the background noise [3].

$$SNR = \frac{\mu}{\sigma} \quad (1)$$

There is no uniform procedure for this method and according to the standard, the manufacturers must determine this themselves. In addition, due to the location-dependent resonances the reproducibility of the measurement results is difficult to achieve. This is illustrated in Fig. 2 which shows the recorded spectrum on the MRI for two different therapy device positions. It can be observed that the intensities (peaks) and their frequency varies significantly. From these general conditions it is clear that an explicit measurement of the disturbance with this method is not possible.

It follows that the aforementioned measuring method is very time consuming and the zipper artifacts are only visible if they fall within the frequency band of the image acquisition. The previously mentioned properties lead to the fact that the results are only valid for a scanner-phantom combination. Due to the combination of poor reproducibility, high effort and no possibility to transfer the results to other scanners, an alternative measurement environment should be considered [3]. Therefore, a statistical method for evaluating interference in the MR environment is proposed in this paper.

A. Reverberation Chamber

A possible alternative for an emission measurement is the evaluation with a reverberation chamber (RVC). The RVC is a test environment from the field of electromagnetic compatibility in which the highly conductive walls and ceilings form a cavity resonator. In that chamber, a so-called mode stirrer ensures a statistically isotropic and homogeneous field distribution. This allows the direct measurement of the radiated power of the device [6]. Furthermore, this method has the advantage that the measurement results can be transferred via the quality factor Q to other shielding cabins. In addition, the MR shielded cabin shows similar boundary

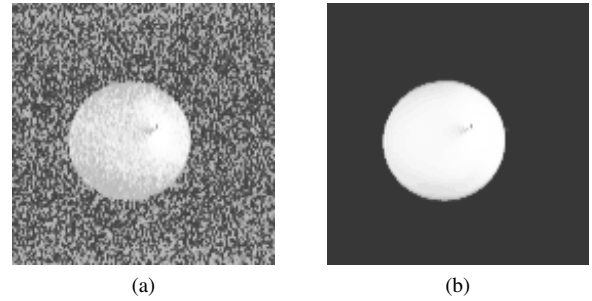


Fig. 3: Slice images to calculate the SNR; Picture (a) shows the disturbed image and Picture (b) the reference

conditions compared to the RVC [3]. The principles of the RVC methods, including the test setup, was transferred to the MR shielded cabin.

III. METHODS

A. Mode Stirrer

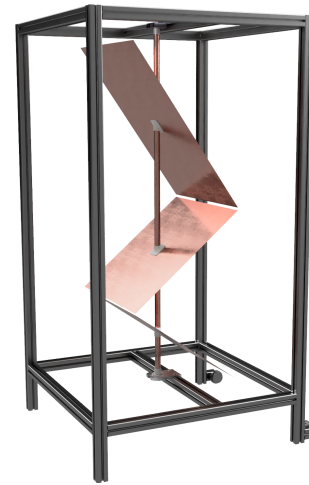


Fig. 4: Developed MR compatible stirrer

TABLE I: Total dimension of the stirrer

Property	Dimension
Height	1.3 m
Width	0.5 m

The MR compatible stirrer in Fig. 4 with the dimensions in Table I was created as part of the research project by Gerhard Jörges [7] and is adapted for this work. Any material used is non-ferromagnetic to allow unrestricted use in the MR environment. Moreover, the plates of the stirrer are made of copper which is diamagnetic and has high electrical conductivity. To avoid bringing additional electrical lines into the MR-cabin, the stirrer is pneumatically driven. In addition, the stirrer has an optical speed measurement, which makes it possible to regulate the rotation.

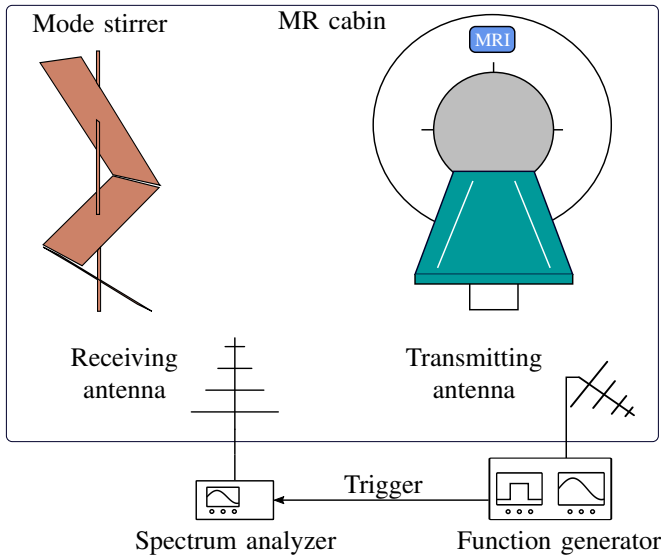


Fig. 5: Test-setup for quality factor Q measurements in the MR cabin

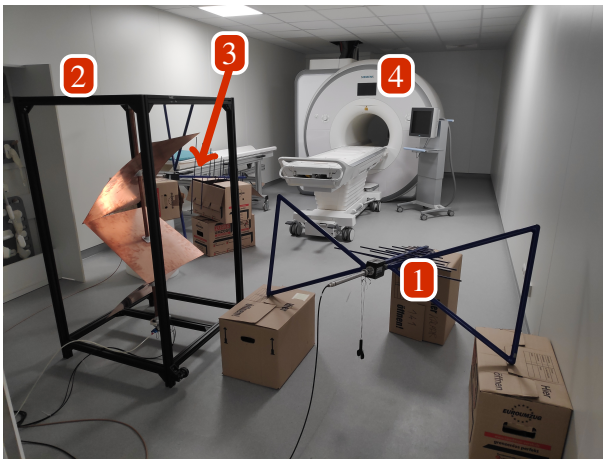


Fig. 6: Measurement setup in the MR-cabin, 1: Transmitting antenna, 2: Mode-stirrer, 3: Receiving antenna and 4: Skyra MRI

B. Quality factor measurement

The setup and principles for the quality factor is based on the bandwidth reduced time domain method from Krauthäuser [8]. The transmitting antenna excites the cavity resonator with a periodic pulsed sinus-signal via the function generator in Fig. 5. When tuned in, the MRI-cabin stores a constant energy. As soon as the excitation is switched off, the energy density will decrease exponentially. This power reduction ΔP and the related time interval Δt can be measured at the base of the receiving antenna [8].

$$Q = \frac{20\pi}{\ln(10)} \cdot f_{\text{MHz}} \cdot \frac{\Delta t_{\text{us}}}{\Delta P_{\text{dB}}} \quad (2)$$

To show the similar measuring conditions between the RVC and the MR shielding cabin, the quality factor has been measured. Therefore, the quality factor of the MRI shielding cabin was measured with the test setup in Fig. 6. This measurement was performed for a frequency range from 20 MHz to 400 MHz, to cover all the Larmor frequencies for commercial available MRIs in the range from 1 T to 7 T. The results are then compared with measurements in the RVC.

C. Emission Measurement

The emission measurement is based on the same principles. In this method the emission from the device under test (DUT) can be acquired by measuring the quality factor Q and the receiving power at the base of the antenna $\langle P_t \rangle$ [8]:

$$\langle P_t \rangle = \frac{4\pi \ln(10) \cdot f^2 \Delta P_{\text{dB}}}{\eta_r 5c^3 \Delta t} \langle P_r \rangle \quad (3)$$

The symbol η describes the antenna efficiency which is approximately 0.75 for logarithmic-periodic antennas. For the chamber volume V , the measurement from the MRI cabin was determined to be 128 m^3 .

To demonstrate the validity of the emission measurement setup, a first device was measured. The used test device is a microwave ablation device (MWA) from MedWaves AveCure (MWG 881, MedWaves Incorporated, San Diego, USA). With the emission setup, the power spectrum of the device in operation is recorded and compared to the power spectrum of the body coil on the 3T MRI.

D. Proof of Concept Measurement

For a first validation of the MR compatible stirrer a first measurement was performed, by generating an interference signal in the center frequency $f_0 = 123\,259\,845\,000 \text{ Hz}$ of the MRI. The frequency spectrum are recorded on a 3T MRI system (Skyra, Siemens, Erlangen, Germany) with the internal body coil which has 2 channels. This measurement was performed for multiple static stirrer positions and then compared with the rotating stirrer. All measurement data were recorded with 16384 frequency points for the frequency range around the Larmor frequency ($123\,259\,845\,000 \text{ Hz} \pm 500 \text{ kHz}$) of the 3T MRI. Each frequency point consists of 1500 measurements, for each of these 1500 measurements the standard deviation of the recorded MRI data set spectrum is calculated.

To proof that the stirrer is statistically varying the position of cables, DUTs (device under test) and also different cable guides etc., a proof of concept measurement was completed. For this reason, a total of 15 emission measurement were recorded on the 3T MRI with different cable guides and device positions. Subsequently, 6 interference emission measurement with the moving stirrer in the cabin was performed. Afterwards, the measurement with the rotating stirrer was compared with the previously recorded variations.

IV. RESULTS

A. Proof of Concept Measurement

In Fig. 7 the standard deviation of the spectra over a complete measurement bandwidth Δf at coil channel 1 of the MRI is shown. It can be noticed that the standard deviation is increasing as soon as the stirrer is in the stirring mode. The averaged standard deviation $\bar{\sigma}$ increases by 7.69% for coil channel 1. From this, it can be concluded that the stirrer has a statistically detectable change of the field distribution in the shielding cabin.

In the evaluation of the 15 variations, the baselines of the recorded frequency spectra were examined. For this purpose, a polynomial interpolation was determined for each recorded spectra. Subsequently, the baseline for the variation measurements was averaged and compared with the averaged 6 stirrer measurements. Fig. 8 shows the results. When comparing, it is visible that the baselines of the spectra show only slight deviations. The spectra were then compared for minima and maxima. From all 15 variation measurements, the maximum and the minimum for each frequency point were calculated and then inserted into global maxima and minima. This was also done for the 6 stirrer measurements. The results are plotted in Fig. 9. When comparing the stirrer maxima and variations maxima, it is noticeable that they are close to each other and are in the same numerical range. The same is also the case when comparing the minima. However, it is noticeable that the minima of the variation measurements are smaller and the maxima of the variation measurements are larger compared to the stirrer measurements, which will be discussed in section V.

B. Quality Factor Measurements

In Fig. 10 the quality factor of the shielding cabin is compared to a absorber loaded RVC [3]. It can be seen that both quality factors rise with increasing frequency. For the frequency range of 100 MHz to 140 MHz, the shielding

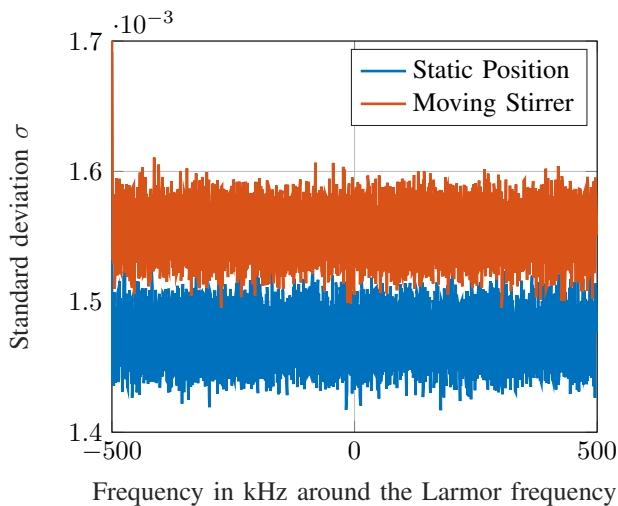


Fig. 7: Standard deviation for the first coil channel of the 3T MRI

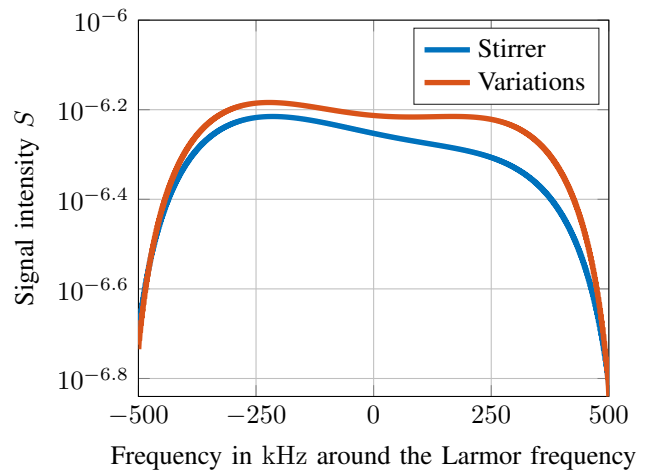


Fig. 8: Comparison of the base line from the measurements

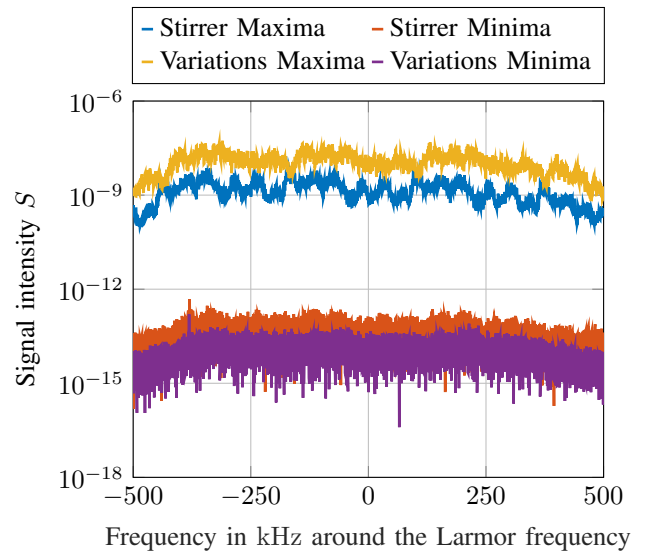


Fig. 9: Comparison of the maximum (upper charts) and minimum from the variations and stirrer measurements

cabin has got a higher quality factor compared to the RVC. At higher frequencies ($f \rightarrow$ Larmor frequency 7 T) the RVC shows a stronger increase.

C. Measuring the Emission

Since the system internal exact voltage values of the Skyra 3 T-MRI are not known, no reception correction is performed and a resistance of $R = 50 \Omega$ is assumed to calculate the power spectrum from the MR data.

When comparing the power spectra in Fig. 11 qualitatively, it is noticeable that the MR data P_{mr} and the data from the emission setup $P_{\text{сна}}$ are almost identical. The difference in value between the two spectra is a constant factor of approximately 30 dBm.

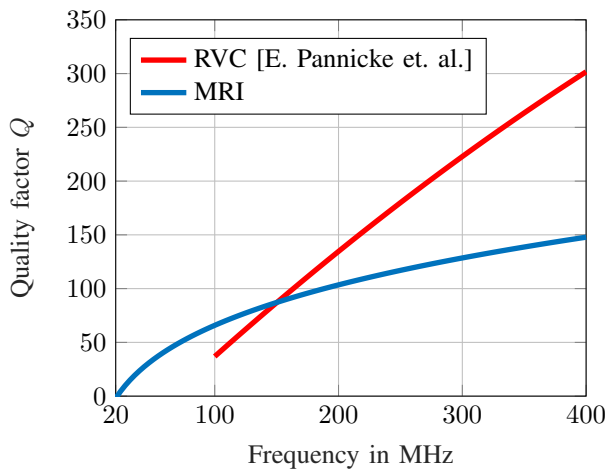


Fig. 10: Comparison of the quality factor Q in the RVC and the MR-cabin

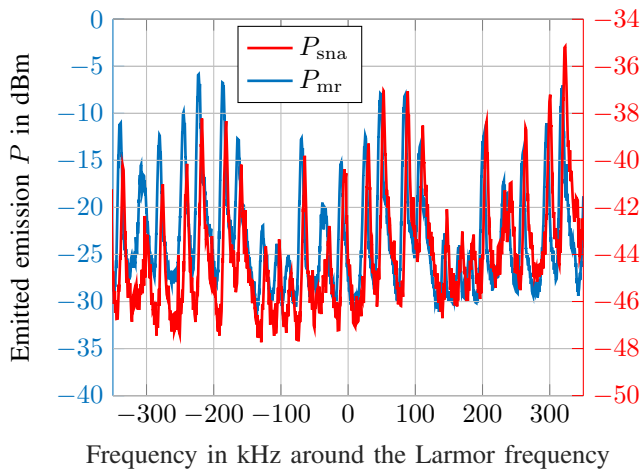


Fig. 11: Calculated radiated power in ablation mode

V. DISCUSSION

One reason for the difference of the quality factor between RVC and the MR-cabin is the shielding cabin material. In a RVC copper or galvanized steel is used which has a higher electrical conductivity κ . Another reason is the loading of the MR cabin by absorbing material. An example for this is the PVC floor and the wooden panels on the walls, which limit the resonance capability of the system. This is one of the main reasons for the lower quality factor in the upper frequency range compared to the RVC. The wall losses are the dominating loss factor in the upper frequency range [6]. In the proof of concept measurement, the comparison of the statistical variation with the variations shows that the results are comparable. It is demonstrated, that the stirrer statically varying DUT positions and cable guides. Despite the good results, the stirring efficiency is not yet known, and might be too small when evaluating the results from section III-D, especially the difference of stirrer measurements to the variations in Fig. 9. The stirring efficiency could be

improved by operating a second stirrer in the shielding cabin or by optimizing the current design [9]. The shown comparability and reproducibility are important properties, as this is difficult to achieve with the *State of The Art* method explained in section II.

In the emission measurement in Fig. 3 a constant difference can be observed. Which is a result from an internal processing by an amplifier chain of the MRI-system, which is not known. By recording the radiated power and later correlating it with the imaging, it is possible to transfer the measurement results to other scanners and shielding cabins. For this, however, the quality factor Q of the shielded cabin must be determined.

VI. CONCLUSION

The subsequent qualitative agreement of test results at the test setup and MRI shows that the developed setup is suitable to perform interference emission measurements in the shielded enclosure. Future works will perform the measurements in different MR cabins to prove the transferability and predictability of this method.

Moreover, the stirrer efficiency will be measured for the frequency bandwidths around the Larmor frequencies for 1.5 T to 7 T. This will be measured by the autocorrelation coefficient of the stirrer positions in order to show the statistically independent field distribution for different stirrer positions.

ACKNOWLEDGMENT

The work of this paper is funded by the federal government of Saxony Anhalt under the operation number FKZ: I 117.

REFERENCES

- [1] S. Heckl, G. C. Feigl, J. Honegger, M. Schumann, M. Horgler, M. Tatagiba, and U. Ernemann, "Intraoperative MRT (iMRT) in der Neurochirurgie: eine radiologische Sichtweise," *RoFo : Fortschritte auf dem Gebiete der Rontgenstrahlen und der Nuklearmedizin*, vol. 184, no. 1, pp. 1–5, 2012.
- [2] U. Kägebein, O. Speck, F. Wacker, and B. Hensen, "Motion Correction in Proton Resonance Frequency-based Thermometry in the Liver," *Topics in magnetic resonance imaging : TMRI*, vol. 27, no. 1, pp. 53–61, 2018.
- [3] E. Pannicke, M. Magdowski, and R. Vick, "Die Modenverwirbelungskammer als alternative Messumgebung für Kompatibilitätstest in der Magnetresonanztomographie," 2018.
- [4] D. W. Harberts, M. van Helvoort, *International Symposium on Electromagnetic Compatibility (EMC Europe), 2014: 1 - 4 Sept. 2014, Gothenburg, Sweden*. Piscataway, NJ: IEEE, 2014.
- [5] B. Gambal, E. Pannicke, M. Magdowski, and R. Vick, "Konzeptionierung und Implementierung eines Prüfverfahrens zur Evaluierung von Störeinkopplungen in der Magnetresonanztomographie," 2020.
- [6] H. G. Krauthäuser, "Grundlagen und Anwendungen von Modenverwirbelungskammern,"
- [7] G. Jörges, "Konzeptstudie zu einem MR-kompatiblen Rührer," 2020.
- [8] H. G. Krauthäuser and J. Nitsch, "Transient Fields in Mode-Stirred Chambers,"
- [9] F. Moglie and V. M. Primiani, "Evaluation of uncorrelation and statistics inside a reverberation chamber in presence of two independent stirrers," in *2010 IEEE International Symposium on Electromagnetic Compatibility*, pp. 515–519, IEEE, 25.07.2010 - 30.07.2010.